

# Characterization of the Uncertainty of the Robertson and Wride Model for Reliability Analysis of Soil Liquefaction

C. Hsein Juang\* and Susan Hui Yang

Department of Civil Engineering

Clemson University

Clemson, SC 29634-0991, USA

Ph: (864) 656-3322; Fax: (864) 656-2670

E-mails: [Hsein@clemson.edu](mailto:Hsein@clemson.edu) (Juang); [yangh@clemson.edu](mailto:yangh@clemson.edu) (Yang)

\*Corresponding author

## ABSTRACT

As the profession moves toward the performance-based earthquake engineering design, it becomes more important and pressing to examine the uncertainty of the limit state model used for liquefaction potential evaluation. In this paper, the uncertainty of the Robertson and Wride model, a simplified model for liquefaction resistance and potential evaluation based on cone penetration test, is investigated in detail for its model uncertainty in the framework of first-order reliability analysis (FORM). The uncertainties of the parameters used in the Robertson and Wride model are also examined. The model uncertainty is characterized using a Bayesian mapping function that is *calibrated* with a fairly large set of case histories. The Bayesian mapping function is created after a series of reliability analyses assuming the parameter uncertainties are at a “reference” level, the reliability analysis at which is termed “baseline analysis.” The results show that the uncertainty of the Robertson and Wride model can be characterized with a mean-to-nominal of 0.94 and a coefficient of variation of 0.15.

**Key words:** Reliability, probability, liquefaction, earthquake, and cone penetration test.

## INTRODUCTION

Soil liquefaction induced by an earthquake can be a major cause of damage to structures and facilities. Whereas much research has been performed over the past three decades to advance the techniques for assessing liquefaction potential of soils, the “simplified procedure” (Seed and Idriss [1]) is still the most widely used method in North America and throughout much of the world. A recent update of the simplified procedure is provided by Youd et al. [2].

The simplified procedure was created initially based on extensive laboratory studies of the behaviors of soils subjected to cyclic loading, and later confirmed and supplemented with field case histories. As more and more case histories of soil liquefaction at sites with in situ testing became available, the simplified procedure was updated accordingly and became known in its present form, in which the “liquefaction loading” is expressed as Cyclic Stress Ratio (CSR) and the “liquefaction resistance” is expressed as Cyclic Resistance ratio (CRR). In a *typical* simplified method, a method that follows the general approach of the simplified procedure created by Seed and Idriss [1], a boundary curve that separates liquefied cases from non-liquefied cases is established and used as a basis for evaluating liquefaction potential. This boundary curve may be expressed symbolically as:  $CRR = f(\text{in situ test index})$ , where the index may be the blow count from Standard Penetration Test (SPT), the normalized cone resistance from Cone Penetration Test (CPT) or the shear wave velocity. Here, the boundary curve is seen as a CRR model. To evaluate liquefaction potential of a soil under a given seismic load, CSR and CRR are calculated, followed by the determination of factor of safety ( $F_s$ ), which is defined as  $F_s = CRR/CSR$ . No liquefaction is predicted if  $F_s > 1$ , and on the

other hand, if  $F_s \leq 1$ , liquefaction is predicted. The evaluation of liquefaction potential using the notion of the factor of safety is generally known as a deterministic approach.

All typical simplified methods use the Seed and Idriss' formulation [1, 2] for CSR, and thus, the differences among the various simplified methods exist only in the way CRR is calculated. Furthermore, in these simplified methods, the boundary curve or the CRR model is generally established through some *calibration* process that uses CSR as a reference. Thus, although CRR may be expressed as a function of only some index of a soil, its measure of "liquefaction resistance" makes sense only in the context of the adopted CSR formulation.

Because the existing boundary curves or CRR models are generally established with a great deal of subjectivity and an unknown degree of conservatism, it would be of interest and importance to assess the uncertainty of these models. This is particularly important if a rigorous reliability analysis, which requires knowledge of both model and parameter uncertainties, is to be conducted. Because of the concern of the uncertainties that are associated with a simplified model and its input parameters, it is prudent to conduct a rigorous reliability analysis that accounts for these uncertainties. The probability of liquefaction obtained from the reliability analysis provides a basis for making performance-based earthquake engineering decision.

Many investigators have employed statistical and probabilistic methods for assessing liquefaction. For example, Haldar and Tang [3] performed second-moment analyses of the SPT-based limit state established by Seed and Idriss [1]. Liao et al. [4] used statistical regression methods to quantify the probability of liquefaction as a function of given earthquake load and SPT blow count. Juang et al. [5, 6] developed a different approach to characterize the deterministic model, in which Bayes' theorem was used to map the calculated

safety index, such as reliability index ( $\beta$ ) or factor of safety ( $F_S$ ), to the probability of liquefaction ( $P_L$ ). None of the aforementioned methods, however, specifically addressed the issue of model uncertainty, the uncertainty of a limit state model.

In this paper, the issue of model uncertainty is addressed and the probability of liquefaction is determined through a rigorous reliability analysis using the First-Order Reliability Method (FORM) that considers model uncertainty. The focus of the paper is on the characterization of the uncertainty of the Robertson and Wride model [7], which is a simplified method for liquefaction resistance based on cone penetration test (CPT). The Robertson and Wride model is used herein as an example to demonstrate the proposed methodology for estimating the model uncertainty that is required in a reliability analysis using FORM.

## **ROBERTSON AND WRIDE MODEL AND LIMIT STATE**

In the context of the reliability analysis presented herein, the boundary curve in a typical simplified method is a limit state. Mathematically, the limit state is defined as:  $g(x_1, x_2, \dots, x_n) = CRR - CSR$ , where  $x_1, x_2, \dots$ , and  $x_n$  are input variables that are required for determining CSR and CRR. As with any typical simplified method, CSR is calculated in the Robertson and Wride model as [1]:

$$CSR_{7.5} = 0.65 \left( \frac{\sigma_v}{\sigma'_v} \right) \left( \frac{a_{\max}}{g} \right) (r_d) / MSF \quad (1)$$

$\sigma_v$  = the vertical total stress of the soil at the depth considered,

$\sigma'_v$  = the vertical effective stress of the soil at the same depth,

$a_{\max}$  = the peak horizontal ground surface acceleration,

$g$  = the acceleration of gravity,

$r_d$  = the shear stress reduction factor, and

MSF = the magnitude scaling factor.

It should be noted that MSF was not included in the original equation by Seed and Idriss [1]; rather, it was used to “scale” CRR. In the present study, it is added to Equation 1 so that CSR is adjusted to an earthquake magnitude of 7.5. Nevertheless, the two approaches result in the same factor of safety. The reader is referred to Youd et al. [2] for details concerning the variables MSF and  $r_d$ .

Needless to say, significant uncertainty exists in this CSR model. However, the uncertainty in the CSR model is “muted” by the fact that the calculated CSR is subsequently used as a reference in the development of CRR model through calibration with field cases, and thus, whatever uncertainty there is in CSR is passed along to the uncertainty in CRR. In other words, in a deterministic approach for assessing liquefaction potential, in which CRR is compared to CSR for judging whether liquefaction will occur, the model uncertainty that needs to be considered is the uncertainty in the CRR model alone.

In the Robertson and Wride model, CRR is calculated as [7]:

$$CRR_{7.5} = 93(q_{c1N,cs}/1000)^3 + 0.08, \text{ if } 50 \leq q_{c1N,cs} < 160 \quad (2a)$$

$$CRR_{7.5} = 0.833(q_{c1N,cs}/1000) + 0.05, \text{ if } q_{c1N,cs} < 50 \quad (2b)$$

where  $q_{c1N,cs}$  is the clean sand equivalence of the stress-corrected cone tip resistance [7], which is a function of the basic parameters,  $q_c$ ,  $f_s$ ,  $\sigma_v$ , and  $\sigma_v'$ . In the Robertson and Wride model, a comprehensive procedure is used to determine  $q_{c1N,cs}$  through the use of some intermediate parameters, including the normalized cone tip resistance ( $q_{c1N}$ ) and the soil behavior index ( $I_c$ ), which are functions of the four basic parameters. According to Robertson and Wride [7], when using Equation 2 in conjunction with Equation 1 for liquefaction potential evaluation, the limiting value of  $q_{c1N,cs}$  is 160 beyond which liquefaction of sandy soils is considered impossible.

#### **FIRST-ORDER RELIABILITY METHOD AND NOTIONAL PROBABILITY**

For reliability analyses presented herein, the Hasofer-Lind reliability index [8] is calculated. In the Hasofer-Lind method, generally known as the advanced first order second moment method (AFOSM), the limit state equation,  $g(x_1, x_2, \dots, x_n) = 0$ , is first transformed to its counterpart in the reduced variable space in which each of the variables has a zero mean and unit standard deviation. The reliability index  $\beta$  is defined as the shortest distance between the limit state surface and the origin in the reduced variable space. Various versions of the AFOSM techniques were proposed, and the more recent versions of the AFOSM techniques became known as First-Order Reliability Method (FORM). FORM requires an optimization algorithm to determine the reliability index. Two types of optimization algorithms are commonly used [9]. One requires solution of the limit state equation during iteration, and the other does not; instead, it uses a Newton-type recursive approach. The latter is used herein because of the complexity of the limit state equation. The reader is referred to the literature

[8-11] for detail regarding the formulation and use of FORM. Once the reliability index is obtained using FORM, the notional probability,  $p_f$ , can be determined as:

$$p_f = 1 - \Phi(\beta) \quad (3)$$

where  $\Phi$  is the standard normal cumulative distribution function (CDF).

### **PARAMETER AND MODEL UNCERTAINTIES**

The limit state is defined herein as:  $g(x_1, x_2, \dots, x_n) = CRR - CSR$ , where  $x_1, x_2, \dots$ , and  $x_n$  are input variables that are required for determining CSR and CRR. These input variables and the associated uncertainty characteristics are described in this section. Each input variable is assumed to follow a lognormal distribution, which has been shown to provide a better fit to the measured geotechnical parameters [12]. A lognormal distribution requires knowledge of the mean and standard deviation. Parameter uncertainty, the uncertainty that is associated with randomness of an input variable, is characterized herein only with its coefficient of variation (COV), since the mean to “nominal” is generally assumed to be 1 in the geotechnical practice. In the CSR model (Equation 1), the variable  $r_d$  is a function of depth ( $z$ ) and is not considered as a random variable (since CSR is evaluated for a soil at a given  $z$ ), although it is recognized that uncertainty does exist in the model for  $r_d$ . As noted previously, the model uncertainty associated with the CSR model and its components such as  $r_d$  and MSF will be accounted for in the CRR model. The variable MSF is a function of  $M_w$ ; thus, the latter ( $M_w$ ) is considered as a random variable. The other variables in the CSR model,  $\sigma_v$ ,  $\sigma_v'$ , and  $a_{max}$ , are also considered as random variables.

In the present study, the COVs for  $\sigma_v$  and  $\sigma_v'$  are taken as 0.10 and 0.15, respectively [6]. The COV for  $M_w$  for all cases is taken as 0.05, whereas the COV for  $a_{\max}$  is taken as 0.10 [13, 14]. These COVs are considered appropriate for reliability analyses of the case histories in the database. It should be noted that the reliability index is calculated herein for a given seismic event at a given site. This should not be confused with a general liquefaction risk analysis where the COV of  $a_{\max}$  due to uncertain attenuation relationship could reach as high as 0.50 [3, 6].

In the CRR model (Equation 2), the basic variables include  $q_c$ ,  $f_s$ ,  $\sigma_v$  and  $\sigma_v'$ . Thus, together with those considered in the CSR model, there are 6 random variables in the limit state function. Thus,  $g(\cdot) = CRR - CSR = g(q_c, f_s, \sigma_v, \sigma_v', a_{\max}, M_w)$ . In the reliability analyses presented herein, the COVs for  $q_c$  and  $f_s$  are assumed to be 0.08 and 0.12, respectively [15]. In practice, however, if the COVs for any input variables at a site differ significantly from those assumed in the analysis presented herein, the site-specific COVs should be used. To this end, it would be of interest to investigate the effect of the level of parameter uncertainty on the calculated reliability index. Reliability analysis using the COVs for the 6 input variables described previously is referred to herein as the *baseline* analysis, as it serves as a reference for other analyses. Investigation of the effect of the level of parameter uncertainty is one focus of the present study, and the results are presented later.

The main focus of the present study is the issue of model uncertainty in the framework of FORM. The model uncertainty is generally difficult to assess, and so is the effect of the model uncertainty on the calculated reliability index and probability of liquefaction. As noted previously, the effect of the uncertainty associated with the CSR model is realized in the CRR

model, and thus, when the model uncertainty is explicitly considered, the limit state function may be expressed as:

$$g() = c_1 \text{CRR} - \text{CSR} = g(c_1, q_c, f_s, \sigma_v, \sigma_v', a_{\max}, M_w) \quad (4)$$

where  $c_1$  is a random variable denoting model uncertainty. Here, the model uncertainty is treated as one additional random variable ( $c_1$ ) in the limit state function. In the present study,  $c_1$  is assumed to follow lognormal distribution. With the assumption of a lognormal distribution, the model uncertainty may be characterized with a mean and a COV. The mean of  $c_1$ , referred to herein as *mean-to-nominal*, is the mean of the ratio of true CRR over predicted CRR (i.e., the CRR calculated with Equation 2). Because the true CRR for each case in the database is generally unknown, it is difficult to estimate the mean of  $c_1$ . In this study, the model uncertainty is investigated with the aid of Bayesian mapping. In addition, parametric analyses with various scenarios of the mean and COV of  $c_1$  are conducted to investigate the effect of model uncertainty in the framework of FORM.

Another issue needs to be considered in the reliability analysis is the correlation among the six input variables. In the present study, except the pair of  $a_{\max}$  and  $M_w$ , the correlation coefficient between each pair of the variables appeared in the limit state function is estimated based on a correlation analysis of the actual data in the database. The correlation coefficient between  $a_{\max}$  and  $M_w$  is taken to be 0.9 [6], which was based on statistical analysis of the data generated from attenuation relationships [16,17]. The coefficients of correlation among the 6 input variables are shown in Table 1.

## RESULTS OF BASELINE RELIABILITY ANALYSIS AND BAYESIAN CALIBRATION OF RELIABILITY INDEX

The results of the baseline reliability analysis, the analysis using FORM without considering model uncertainty, are presented first. Here, the reliability index  $\beta$  is calculated for each case in the database of 226 case histories [6] using FORM considering all parameter uncertainties as described previously but not the unknown model uncertainty. For each case, the probability of liquefaction ( $P_L$ ) may be interpreted from the calculated reliability index  $\beta$  with the notional probability concept (Equation 3). Figure 1 shows a plot of the notional probabilities versus the calculated  $\beta$  values. Because the model uncertainty was not considered in the analysis, the calculated reliability index and probability of liquefaction may be underestimated or overestimated. Juang et al. [6] showed that the probability of liquefaction could be interpreted for a given  $\beta$  through a calibration with field observations, by means of Bayes' theorem:

$$P_L = P_r(\text{Liq} | \beta) = \frac{f_L(\beta)}{f_L(\beta) + f_{NL}(\beta)} \quad (5)$$

where the probability of liquefaction  $P_L$  is interpreted as a conditional probability,  $P_r(\text{Liq} | \beta)$ , given a calculated  $\beta$ . This probability is a function of  $f_L(\beta)$  and  $f_{NL}(\beta)$ , the probability density functions of the calculated  $\beta$  of the group of liquefied cases and the group of non-liquefied cases, respectively [6]. Thus, for a given  $\beta$  value, the probability ( $P_L$ ) can be determined with Equation 5 that is calibrated to field observations. A plot of  $P_L$ - $\beta$  obtained from this Bayesian mapping approach is also shown in Figure 1.

Discrepancy is observed between the two curves shown in Figure 1. The Bayesian probability curve is calibrated with field data and is considered as the “true” probability or at least a close approximation of the true probability. Whereas the notional probability concept is well established, accuracy of the estimated probability depends on the accuracy of the calculated  $\beta$ . Thus, the model uncertainty must be correctly assessed and incorporated in the reliability analysis using FORM. On the other hand, with Bayesian mapping approach, the estimated probability is calibrated through the reliability index using a fairly large database of field observations, and thus, the effect of model uncertainty, whatever it is, is reflected in the calculated probability. However, if the parameter uncertainty level of a future case differs significantly from that assumed in the baseline analysis, use of the mapping function shown in Figure 1 for estimation of probability may be subjected to error. In such case, use of FORM, which can easily be adjusted to consider the actual parameter uncertainties, is preferred, provided that the model uncertainty has been pre-determined.

### **Effect of the Level of Parameter Uncertainty**

The effect of the level of parameter uncertainty may be investigated by comparing the Bayesian mapping function obtained for each uncertainty level. Figure 2 shows the effect of the uncertainty level of the parameter  $q_c$  alone. Here, three levels of uncertainty, reflected by different COVs (0.08, 0.15, and 0.20), are assumed in the reliability analysis using FORM. For these analyses, the COVs for all other variables are maintained at the same level as in the baseline analyses. The  $\beta$  values for all cases in the database are calculated with each assumed COV of  $q_c$ , and the Bayesian mapping approach is used to establish the  $P_L$ - $\beta$  relationship. The results show that within some range of COV (from COV = 0.08 to 0.15) the level of  $q_c$

uncertainty has little effect on the  $P_L$ - $\beta$  relationship (i.e., Bayesian mapping function); however, the effect becomes significant at a greater COV value.

Similarly, the effect of the uncertainty of  $f_s$  is examined and shown in Figure 3. Here, three levels of uncertainty, in terms of COVs (0.12, 0.25, and 0.35), are assumed in the reliability analysis. Significant difference is observed between the cases of COV = 0.12 and COV= 0.25, but not much difference between the cases of COV = 0.25 and COV= 0.35.

Similar sensitivity analyses are also performed to investigate the effect of the level of uncertainty of  $a_{max}$  and  $M_w$ . Four different scenarios are considered: (1) COV\_ $a_{max}$  (the COV of  $a_{max}$ ) = 0.1 and COV\_ $M_w$  (the COV of  $M_w$ ) = 0.05, (2) COV\_ $a_{max}$  = 0.3 and COV\_ $M_w$  = 0.05, (3) COV\_ $a_{max}$  = 0.5 and COV\_ $M_w$  = 0.05, and (4) COV\_ $a_{max}$  = 0.5 and COV\_ $M_w$  = 0.1. Figure 4 shows the results of the analysis, which indicate that as the COV of  $a_{max}$  increases, there is significant change in the  $P_L$ - $\beta$  curve; the effect of  $M_w$  uncertainty is not as significant.

The results of the above sensitivity analyses suggest that the  $P_L$ - $\beta$  mapping function developed from the baseline analysis may not be applicable if the actual parameter uncertainty of a future case differs significantly from those assumed in the baseline analysis. Since it is not practical to develop a  $P_L$ - $\beta$  mapping function for each of a large number of different possible scenarios of parameter uncertainties, a rigor reliability analysis using FORM is considered a better approach to estimation of the probability of liquefaction, provided that the model and parameter uncertainties have been predetermined.

## **ESTIMATION OF MODEL UNCERTAINTY**

To focus on the uncertainty of the Robertson and Wride model, the parameter uncertainty in the reliability analyses presented in this section is kept at the same level as in

the baseline reliability analysis. As noted previously, at the level of parameter uncertainty assumed in the baseline analysis, the Bayesian mapping function obtained through calibration with field observations, shown in Figure 1, yields a close approximation of the true probability of liquefaction. Thus, the obtained Bayesian mapping function may be used to estimate the uncertainty of the Robertson and Wride model. This can be carried out by conducting a series of reliability analyses using FORM that incorporates different levels of model uncertainty.

As noted previously, the model uncertainty is implemented with a random variable  $c_1$  in Equation 4. For convenience, the reliability index calculated from the previous analyses that did not consider model uncertainty is denoted as  $\beta_1$ , and the reliability index calculated considering model uncertainty is denoted as  $\beta_3$ . Using the  $P_L$ - $\beta$  relationship obtained from Bayesian mapping, as depicted in Figure 1, the probability of liquefaction can be determined for each calculated  $\beta_1$  value. The probability that corresponds to  $\beta_1$  is denoted as  $P_{L1}$ , which is an accurate estimate of the probability, as it has been calibrated with field observations. On the other hand, the probability of liquefaction that corresponds to  $\beta_3$ , denoted herein as  $P_{L3}$ , is a notional probability (Equation 3). If the model and parameter uncertainties are accurately assessed, the reliability index obtained from FORM will be accurate and so will be the probability of liquefaction. In such cases, it is expected that  $P_{L1} \approx P_{L3}$ .

Figure 5 shows a comparison of  $\beta_3$  with  $\beta_1$  for all cases analyzed, where  $\beta_3$  were obtained with four scenarios, (a) the mean of  $c_1$ , denoted as  $\mu_{c1}$ , is equal to 0.8, and the COV of  $c_1$ , is equal to 10%, (b)  $\mu_{c1} = 0.9$ , COV = 10%, (c)  $\mu_{c1} = 1.0$ , and COV = 10%, and (d)  $\mu_{c1} = 1.2$ , and COV = 10%. It should be noted that the results with a COV of 10% is presented herein as an example; other levels of COV have also been investigated and similar

conclusions are reached. This series of analyses is to investigate the effect of  $\mu_{c1}$  component of the model uncertainty, which is reflected in the change in the intercept of the linear trend line of the plot of  $\beta_3$  versus  $\beta_1$ . As  $\mu_{c1}$  increases, the calculated reliability index  $\beta_3$  increases, which is expected, as a higher  $\mu_{c1}$  value implies a more conservative “limit state” model, and thus, the reliability analysis that considers this model uncertainty should yield a higher reliability index.

Similarly, Figure 6 shows a comparison of  $\beta_3$  with  $\beta_1$  for all cases analyzed, where  $\beta_3$  were obtained with four scenarios, (a)  $\mu_{c1} = 1.0$  and  $COV = 0$ , (b)  $\mu_{c1} = 1.0$  and  $COV = 10\%$ , (c)  $\mu_{c1} = 1.0$  and  $COV = 15\%$ , and (d)  $\mu_{c1} = 1.0$  and  $COV = 20\%$ . This series of analyses is to investigate the effect of  $COV$  component of the model uncertainty. The scenario with  $\mu_{c1} = 1.0$  and  $COV = 0$  is essentially the same as the analysis without considering model uncertainty, and thus,  $\beta_3 = \beta_1$  for all cases analyzed. The effect of  $COV$  component is reflected in the decreasing slope of the linear trend line of the plot of  $\beta_3$  versus  $\beta_1$ . As the  $COV$  increases, the calculated reliability index  $\beta_3$  decreases, which is consistent with the well-established reliability theory.

As noted previously, the notional probabilities based on  $\beta_3$  that were obtained using FORM,  $P_{L3}$ , are expected to be approximately equal to  $P_{L1}$ , the probability of liquefaction determined from the Bayesian mapping function that was developed based on  $\beta_1$ , provided that the model and parameter uncertainties are accurately assessed. Figure 7 compares  $P_{L3}$  with  $P_{L1}$ , where  $P_{L3}$  and  $P_{L1}$  are obtained from the corresponding  $\beta_3$  and  $\beta_1$  that are shown in Figure 5. It should be noted that the line in each graph included in Figure 7 is the “perfect match” line where  $P_{L3} = P_{L1}$ . By raising the value of  $\mu_{c1}$ , the trend of  $P_{L3} > P_{L1}$ , observed in

Figure 7(a), is reversed to the trend of  $P_{L3} < P_{L1}$ , observed in Figure 7(d). This trend suggests that there is an optimal  $\mu_{c1}$  value at which  $P_{L3} \approx P_{L1}$ . Thus, it is possible to estimate the model uncertainty based on the results of a Bayesian mapping function that has previously been calibrated with field observations.

Figure 8 shows a plot similar to Figure 7 but with the model uncertainty scenarios corresponding to those shown in Figure 6. The scenario with  $\mu_{c1} = 1.0$  and  $COV = 0$  is essentially the same as the analysis without considering model uncertainty, and thus, for most cases,  $P_{L3} < P_{L1}$ , which is also reflected in Figure 1 discussed previously. As the  $COV$  increases,  $\beta_3$  decreases and  $P_{L3}$  increases. Since  $P_{L1}$  remains the same for each case, the  $P_{L3}$  versus  $P_{L1}$  curves move up and closer to the “perfect match” line. The effect of  $COV$ , however, is less significant, as reflected in the “trend” revealed in Figure 8.

The importance and need to strive for a realistic estimate of both components of the model uncertainty, particularly the  $\mu_{c1}$  component, which is generally more difficult to estimate, is evidenced from the results shown in Figures 5 and 6, and again, in Figures 7 and 8.

Based on the results shown in Figures 7 and 8, a series of reliability analyses with various combinations of  $COV$  and  $\mu_{c1}$  are carried out to “fine-tune” the level of uncertainty so that the best match between  $P_{L3}$  and  $P_{L1}$  is obtained. Figure 9 shows the best match result, which occurs when the model uncertainty is characterized with  $\mu_{c1} = 0.94$  and  $COV = 15\%$ .

The implication of the results shown in Figures 5 through 9 is very significant. First, the robustness of the Bayesian mapping approach is evidenced from the plots of  $\beta_3$  versus  $\beta_1$  and those of  $P_{L3}$  versus  $P_{L1}$ . Second, if the model uncertainty is correctly characterized and explicitly incorporated in the analysis, the accuracy of the reliability index determined by FORM, and that of the corresponding notional probability, can be assured. However, the

reliability analysis using FORM may not yield an accurate estimate of the probability if either or both components of the model uncertainty are not correctly characterized and incorporated in the analysis. Third, in the situation where the fully calibrated Bayesian mapping function is available, as is the case in the present study of soil liquefaction based on field cases, model uncertainty may be evaluated using the Bayesian mapping function.

To further confirm the conclusions reached, all analyses are repeated using a different level of parameter uncertainty. The new level of parameter uncertainty is represented by the COVs of the six parameters,  $\sigma_v$ ,  $\sigma_v'$ ,  $a_{max}$ ,  $M_w$ ,  $q_c$ , and  $f_s$ , which are 0.10, 0.15, 0.10, 0.05, 0.15, and 0.25, respectively. The difference between this set of parameter uncertainty with that used in the previous baseline analysis is that the COVs for  $q_c$  and  $f_s$  are doubled in the new baseline analysis. Under this assumed parameter uncertainty level, a new Bayesian mapping function is obtained after the reliability index for each case in the database is determined with FORM without considering the model uncertainty.

Using the new Bayesian mapping function as a reference, the model uncertainty of the Robertson and Wride model can be estimated following the procedure described previously. Based on the best match between  $P_{L3}$  and  $P_{L1}$  (see Figure 10), the uncertainty of the Robertson and Wride model is *again* characterized with  $\mu_{c1} = 0.94$  and  $COV = 15\%$ .

For prediction of a future case where the actual uncertainties of input variables ( $q_c$ ,  $f_s$ ,  $\sigma_v$ ,  $\sigma_v'$ ,  $a_{max}$ ,  $M_w$ ) are approximately equal to those used in the baseline analysis, both Bayesian mapping approach that does not consider model uncertainty and the FORM approach that considers model uncertainty can be used, and will yield approximately the same result. If the parameter uncertainties differ significantly from those used in the baseline

analysis, the FORM approach is the method of choice, as it can easily accommodate the actual parameter uncertainties in the reliability analysis.

In summary, the uncertainty of the CPT-based simplified model by Robertson and Wride (1998) has been characterized. In the form of Equation 4, the uncertainty of this model can be characterized with  $\mu_{c1} = 0.94$  and  $COV = 15\%$ . This model uncertainty should be incorporated along with the parameter uncertainty into the reliability analysis using FORM.

## CONCLUSIONS

Based on the results presented, the following conclusions are reached in this paper:

1. Uncertainty of the Robertson and Wride model (Equation 2) may be represented with a random variable  $c_1$  that can be characterized with two statistical parameters, the mean ( $\mu_{c1}$ ), and the coefficient of variation (COV). The results show that *both* components of model uncertainty have a significant effect on the calculated reliability indices, although the effect of the  $\mu_{c1}$  component is more significant in this study. Thus, it is important to strive for a realistic estimate of both components of model uncertainty, not just COV, as is usually done in the traditional geotechnical reliability analysis.
2. The first order reliability method is shown to be able to estimate accurately the reliability index and the corresponding probability of liquefaction, if correct parameter and model uncertainties are incorporated in the analysis. Without knowledge of model uncertainty, however, accuracy of the calculated reliability index and the corresponding notional probability may be in question.

3. Robustness of the Bayesian mapping approach to obtain the  $P_L$ - $\beta$  mapping function is demonstrated in this study. In the situation where the fully calibrated Bayesian mapping function is available, as is the case in the present study of soil liquefaction, model uncertainty may be evaluated using the Bayesian mapping function. The Robertson and Wride model is estimated to have a model uncertainty that is characterized with a mean ( $\mu_{c1}$ ) of 0.94 and a COV of 15%. This model uncertainty should be explicitly considered, along with parameter uncertainty, when adopting FORM for reliability analyses of soil liquefaction using CPT.

### **ACKNOWLEDGEMENT**

The study on which this paper is based was supported by the National Science Foundation through Grants No. CMS-0218365. This financial support is greatly appreciated. The opinions presented in this paper, however, do not necessarily reflect the view of the National Science Foundation.

## REFERENCES

- [1] Seed, H.B., and Idriss, I.M. Simplified procedure for evaluating soil liquefaction potential. *Journal of the Soil Mechanics and Foundations Division, ASCE*, 1971; 97 (9): 1249-1273.
- [2] Youd, T. L., Idriss, I. M., Andrus, R.D., Arango, I., Castro, G., Christian, J.T., Dobry, R., Liam Finn, W.D., Harder, L.F., Jr., Hynes, M.E., Ishihara, K., Koester, J.P., Laio, S.S.C., Marcuson, W.F., III, Martin, G.R., Mitchell, J.K., Moriwaki, Y., Power, M.S., Robertson, P.K., Seed, R.B., Stokoe, K.H., II. Liquefaction resistance of soils: summary report from the 1996 NCEER and 1998 NCEER/NSF workshops on evaluation of liquefaction resistance of soils. *Journal of Geotechnical and Geoenvironmental Engineering*, 2001; 127(10): 817-833.
- [3] Haldar, A., and Tang, W.H. Probabilistic evaluation of liquefaction potential. *Journal of Geotechnical Engineering, ASCE*, 1979; 104(2): 145-162.
- [4] Liao, S.S.C., Veneziano, D., and Whitman, R.V. Regression models for evaluating liquefaction probability. *Journal of Geotechnical Engineering, ASCE*, 1988; 114(4): 389-410.
- [5] Juang, C. H., Rosowsky, D.V. and Tang, W.H. A reliability-based method for assessing liquefaction potential of sandy soils. *Journal of Geotechnical and Geoenvironmental Engineering, ASCE*, 1999; 125(8): 684-689.
- [6] Juang, C.H., Chen, C.J., Rosowsky, D.V., and Tang, W.H. CPT-based liquefaction analysis, Part 2: Reliability for design. *Geotechnique*, 2000; 50(5): 593-599.
- [7] Robertson, P.K., and Wride, C.E. Evaluating cyclic liquefaction potential using the cone penetration test. *Canadian Geotechnical Journal*, 1998, 35(3): 442-459.
- [8] Ditlevson, O. *Uncertainty Modeling*, McGraw Hill, New York, 1981.

- [9] Haldar, A. and Mahadevan, S. Probability, Reliability and Statistical Methods in Engineering Design, John Wiley & Sons, New York, 2000.
- [10] Der Kiureghian, A., Lin, H.Z., and Hwang, S.J. Second-order reliability approximations. Journal of Engineering Mechanics, ASCE, 1987; 113(8): 1208-1225.
- [11] Melchers, R.E. Structural Reliability: Analysis and Prediction, Ellis Horwood Limited, distributed by Jogn Wiley & Sons, New York, 1987.
- [12] Jefferies, M.G., Rogers, B.T., Griffin, K.M., and Been, K. Characterization of sandfills with the cone penetration test. Penetration Testing in the UK, Thomas Telford, London, UK, 1988, pp. 199-202.
- [13] Espinosa, A.F. ML and MO determination from strong-motion accelerograms, and expected intensity distribution. The Imperial Valley, California, Earthquake of October 15, 1979, Geological Survey Professional Paper 1254, United States Government Printing Office, Washington, 1982; 433-438.
- [14] Comartin, C.D., Greene, M., and Tubbesing, S.K. The Hyogo-Ken Nanbu Earthquake Preliminary Reconnaissance Report, EERI Report No. 95-40, Earthquake Engineering Research Institute, California, 1995.
- [15] Kulhawy, F.H. and Trautmann, C.H. Estimation of in-situ test uncertainty. Uncertainty in the Geologic Environment: From Theory to Practice, ASCE Geotechnical Special Publication, No. 58, C. D. Shackelford, P. P. Nelson, and M. J. S. Roth, editors, 1996; 269-286.
- [16] Campbell, K.W. Near-surface attenuation of pear ground acceleration. Bulletin of the Seismological Society of America, 1981; 71(6): 2039-2070.

- [17] Idriss, I.M. Earthquake ground motions at soft soil sites. Proceedings, the 2nd International Conference on Recent Advances in Geotechnical Earthquake Engineering and Soil Dynamics, University of Missouri-Rolla, Rolla, MO; 1991; 3: 2265-2271.

Table 1. Coefficients of correlation of the input variables

	$q_c$	$f_s$	$\sigma_v'$	$\sigma_v$	$a_{max}$	$M_w$
$q_c$	1.00	0.37	0.25	0.25	0.00	0.00
$f_s$	0.37	1.00	0.54	0.52	0.00	0.00
$\sigma_v'$	0.25	0.54	1.00	0.93	0.00	0.00
$\sigma_v$	0.25	0.52	0.93	1.00	0.00	0.00
$a_{max}$	0.00	0.00	0.00	0.00	1.00	0.90
$M_w$	0.00	0.00	0.00	0.00	0.90	1.00

Note: All variables are assumed to follow the lognormal distribution.

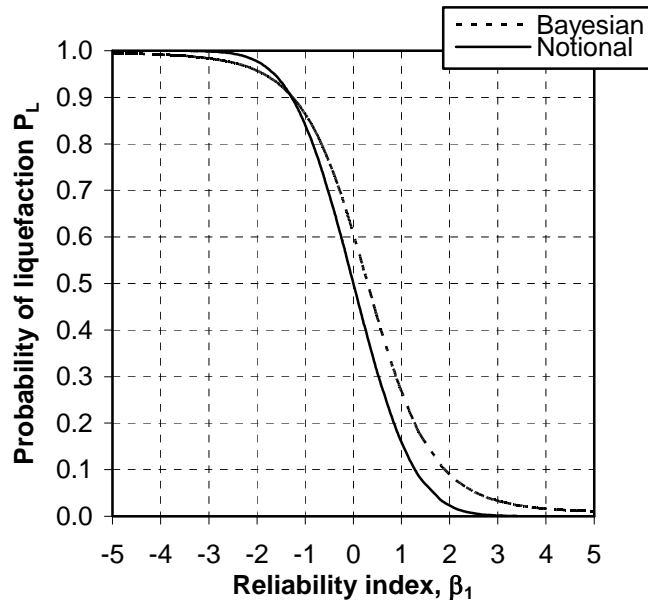


Figure 1. Bayesian probability versus notional probability with reliability indices obtained from the first baseline analysis

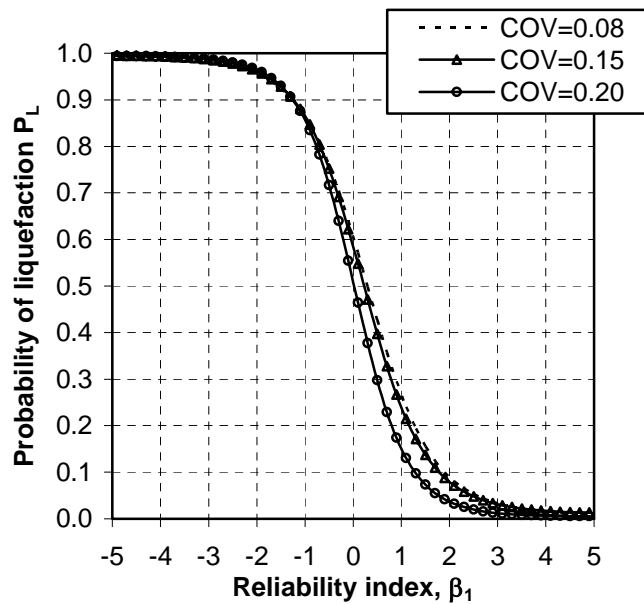


Figure 2. Effect of COV of  $q_c$  on the Bayesian  $P_L - \beta$  relationship

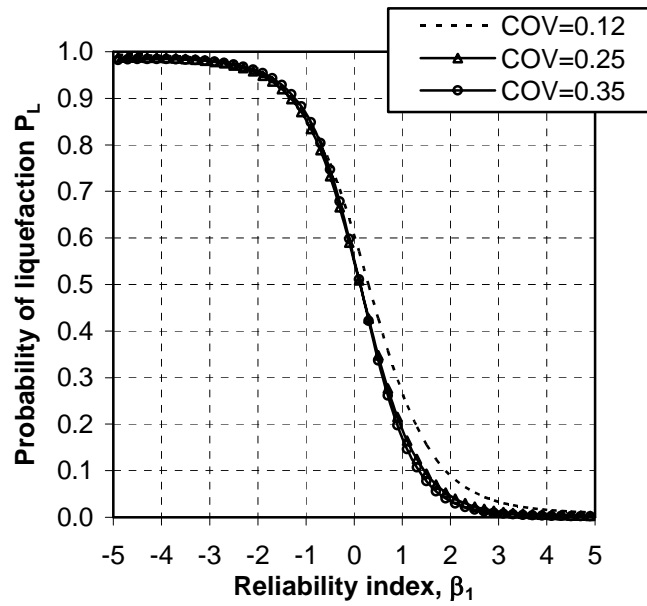


Figure 3. Effect of COV of  $f_s$  on the Bayesian  $P_L - \beta_1$  relationship

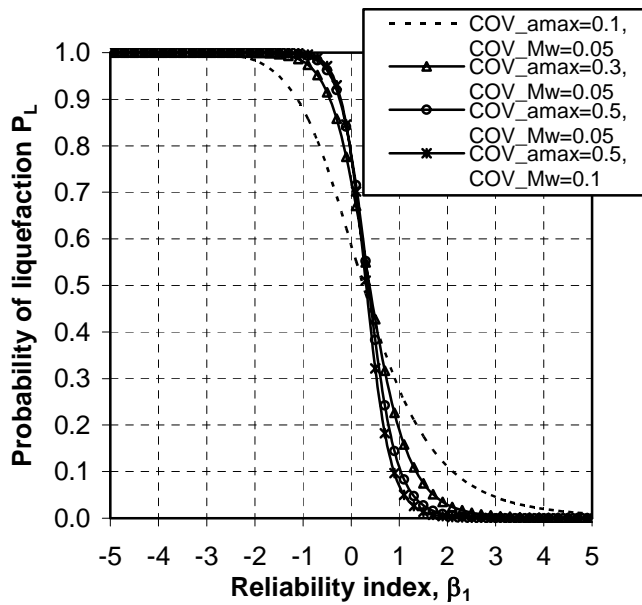
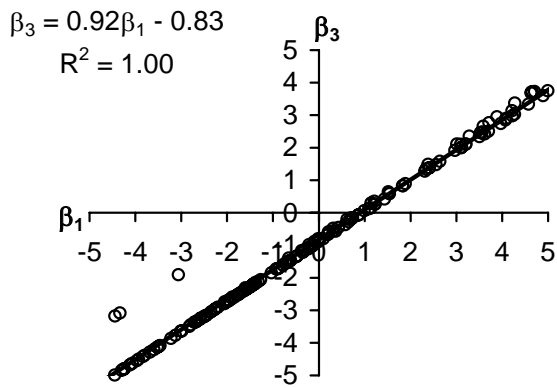
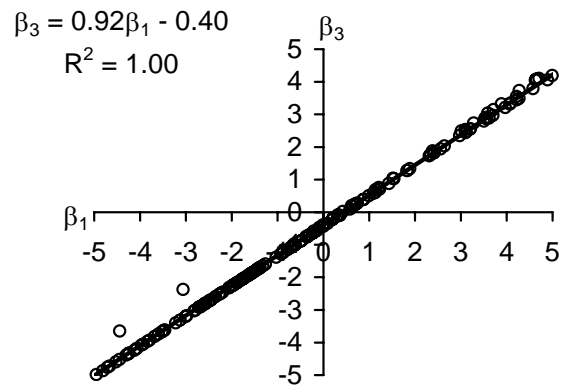


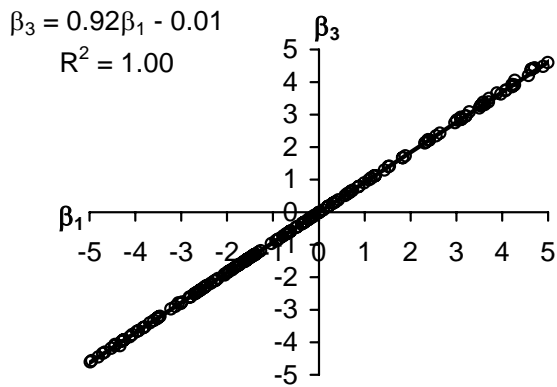
Figure 4. Effect of COVs of  $a_{max}$  and  $M_w$  on the Bayesian  $P_L - \beta_1$  relationship



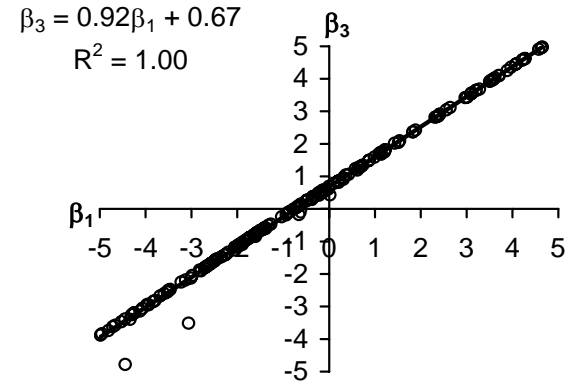
(a)  $\mu_{c1} = 0.8$ , COV = 10%



(b)  $\mu_{c1} = 0.9$ , COV = 10%

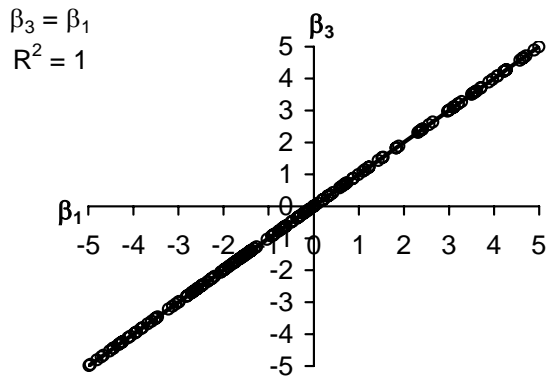


(c)  $\mu_{c1} = 1.0$ , COV = 10%

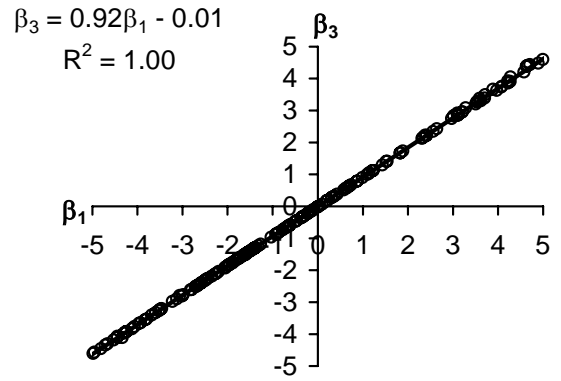


(d)  $\mu_{c1} = 1.2$ , COV = 10%

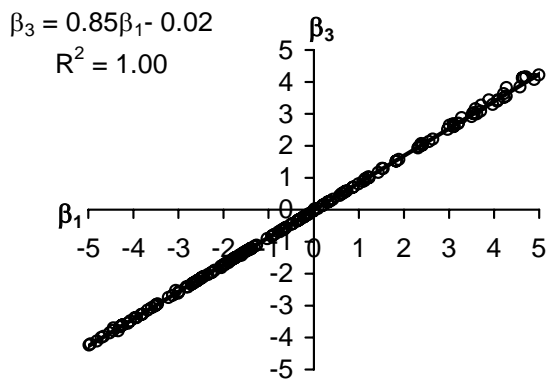
Figure 5. Effect of the  $\mu_{c1}$  component of model uncertainty on the reliability indices



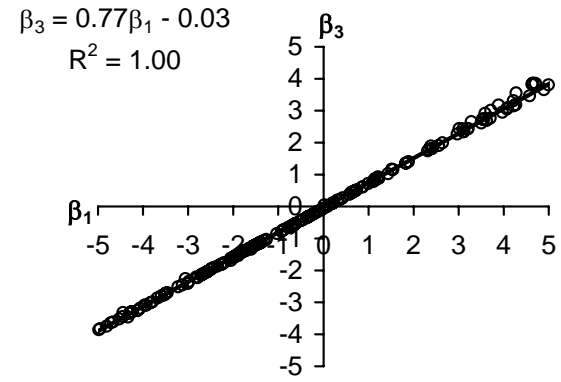
(a)  $\mu_{c1} = 1.0$ , COV = 0



(b)  $\mu_{c1} = 1.0$  COV = 10%

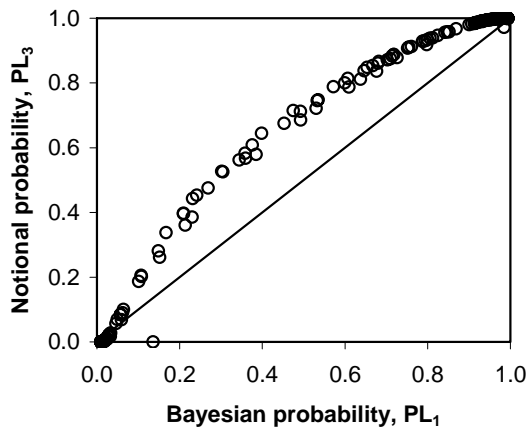


(c)  $\mu_{c1} = 1.0$ , COV = 15%

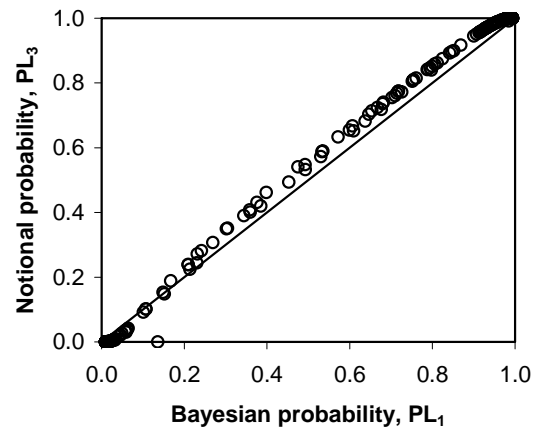


(d)  $\mu_{c1} = 1.0$ , COV = 20%

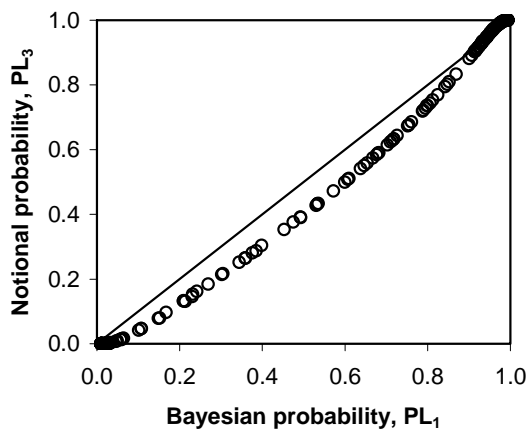
Figure 6. Effect of the COV component of model uncertainty on the reliability indices



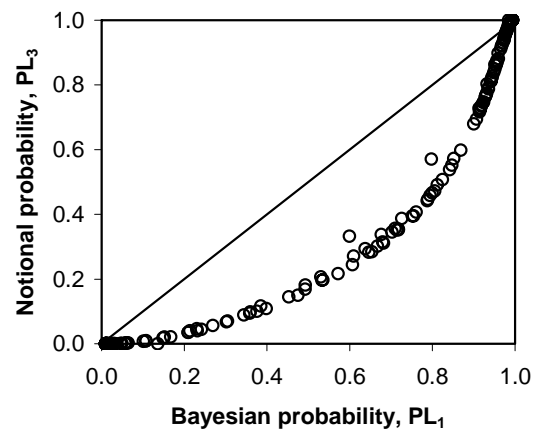
(a)  $\mu_{c1} = 0.8$ , COV = 10%



(b)  $\mu_{c1} = 0.9$ , COV = 10%

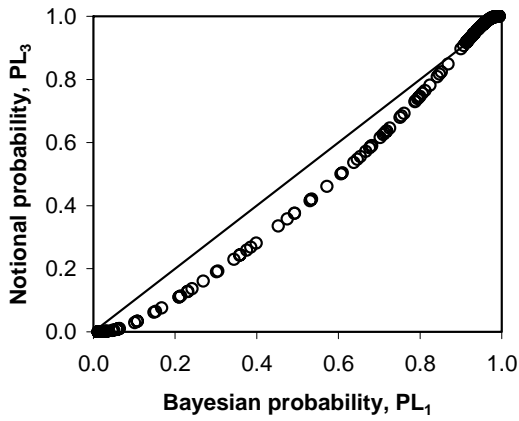


(c)  $\mu_{c1} = 1.0$ , COV = 10%

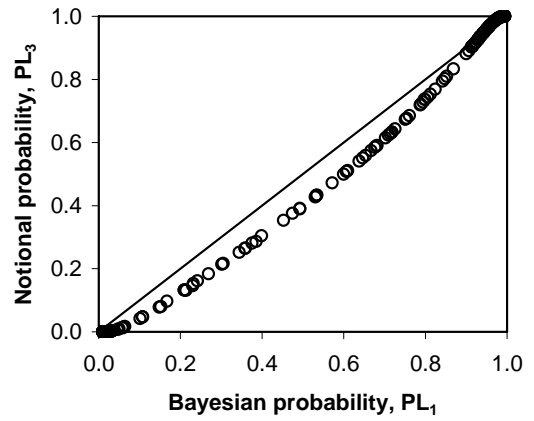


(d)  $\mu_{c1} = 1.2$ , COV = 10%

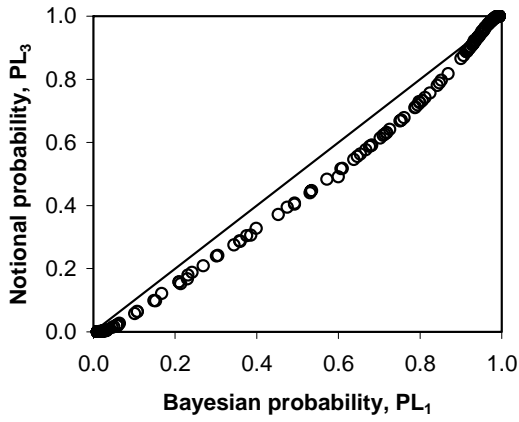
Figure 7. Notional probability based on  $\beta_3$  versus Bayesian probability based on  $\beta_1$  for four scenarios of model uncertainty with varying  $\mu_{c1}$



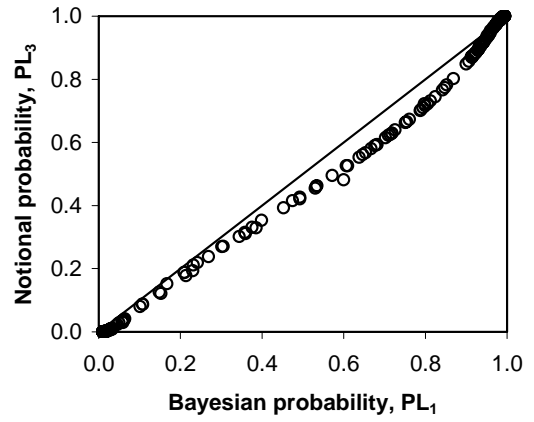
(a)  $\mu_{c1} = 1.0, \text{COV} = 0$



(b)  $\mu_{c1} = 1.0, \text{COV} = 10\%$



(c)  $\mu_{c1} = 1.0, \text{COV} = 15\%$



(d)  $\mu_{c1} = 1.0, \text{COV} = 20\%$

Figure 8. Notional probability based on  $\beta_3$  versus Bayesian probability based on  $\beta_1$  for four scenarios of model uncertainty with varying COV

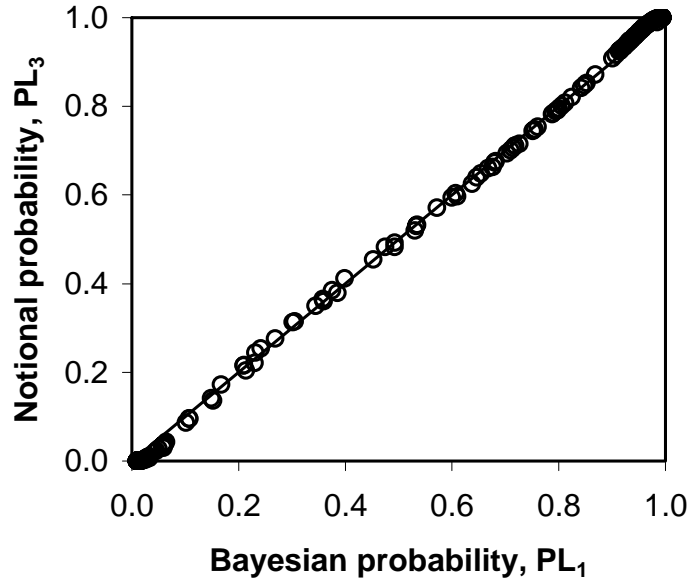


Figure 9. Notional probability versus Bayesian probability (the model uncertainty is characterized by  $\mu_{c1} = 0.94$  and  $COV = 15\%$ , and the parameter uncertainty is at the same level as in the first baseline analysis)

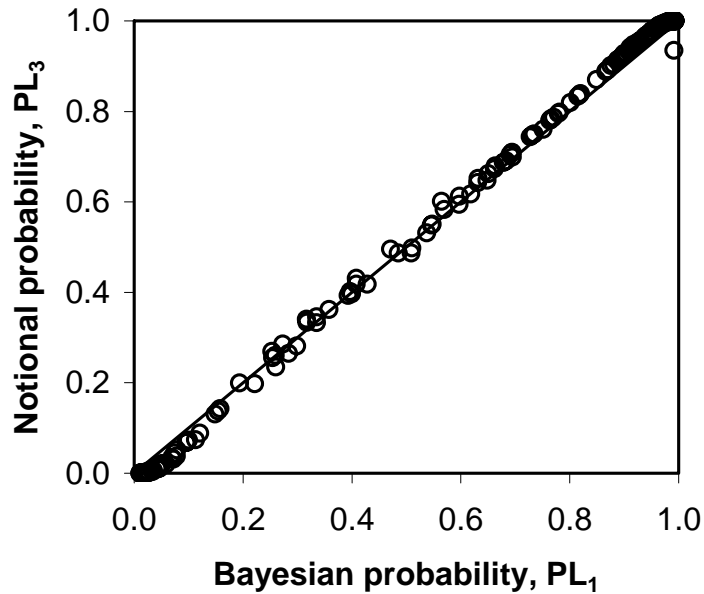


Figure 10. Notional probability versus Bayesian probability (the model uncertainty is characterized by  $\mu_{c1} = 0.94$  and  $COV = 15\%$ , and the parameter uncertainty is at the same level as in the second baseline analysis)